CEPRA - A new test method for rebar corrosion rate measurement

Journal:	*STP: Selected Technical Papers*
Manuscript ID	STP-2017-0227
Manuscript Type:	Full Length Paper
Date Submitted by the Author:	10-Nov-2017
Complete List of Authors:	Fahim, Andrew; University of New Brunswick, Civil Engineering Ghods, Pouria; Giatec Scientific Inc, ; Carleton University, Civil and Environmental engineering Dep. Alizadeh, Rouhollah; Giatec Scientific Salehi, Mustafa; Giatec Scientific Inc Decarufel, Sarah; Giatec Scientific
ASTM Committees and Subcommittees:	G01.11 Electrochemical Measurements in Corrosion Testing < G01 Committee on Corrosion of Metals
Keywords:	Corrosion-monitoring, rebar corrosion, concrete durability, non-destructive testing, connectionless corrosion-monitoring, CEPRA
Abstract:	The corrosion rate of rebar in concrete has been traditionally determined using polarization methods such as the potentiodynamic technique, galvanostatic pulse technique, potentiostatic pulse technique, and, in some cases, the electrochemical impedance spectroscopy technique in laboratory applications. These techniques are very slow and all require having an electrical connection to the rebar which make them impractical in the field. In this paper, the recently-developed technique of Connectionless Electrical Pulse Response Analysis (CEPRA) will be introduced. The CEPRA method, which eliminates the need to have a rebar connection, is based on the concept that the voltage response of the corroding rebar is different from that of the non-corroding rebar once subjected to variable frequencies of an AC current applied on the concrete surface using the four-probe Wenner array configuration. However, direct measurement of the low-frequency impedance of rebar in concrete is very time-consuming and vulnerable to noise interruption; hence, in the CEPRA method a narrow current pulse is applied for a short period of time (in a couple of seconds). Using the recorded voltage and the applied current, the low-frequency impedance response of rebar in concrete can be extracted, which can be used to determine the state of corrosion in reinforced concrete structures. The details of the CEPRA technique and equivalent electrical circuit models will be discussed in this paper. Laboratory and finite element modeling results will be presented to compare the traditional corrosion rate measurement techniques with the CEPRA method.

CEPRA – A New Test Method for Rebar Corrosion Rate Measurement

Andrew Fahim[1], Pouria Ghods[2], Rouhollah Alizadeh[2], Mustafa Salehi[2], Sarah Decarufel[2]

ABSTRACT

The corrosion rate of rebar in concrete has been traditionally determined using polarization methods such as the potentiodynamic technique, galvanostatic pulse technique, potentiostatic pulse technique, and, in some cases, the electrochemical impedance spectroscopy technique in laboratory applications. These techniques are very slow and all require having an electrical connection to the rebar which make them impractical in the field. In this paper, the recently-developed technique of Connectionless Electrical Pulse Response Analysis (CEPRA) will be introduced. The CEPRA method, which eliminates the need to have a rebar connection, is based on the concept that the voltage response of the corroding rebar is different from that of the non-corroding rebar once subjected to variable frequencies of an AC current applied on the concrete surface using the four-probe Wenner array configuration. However, direct measurement of the low-frequency impedance of rebar in concrete is very time-consuming and vulnerable to noise interruption; hence, in the CEPRA method a narrow current pulse is applied for a short period of time (in a couple of seconds). Using the recorded voltage and the applied current, the low-frequency impedance response of rebar in concrete can be extracted, which can be used to determine the state of corrosion in reinforced concrete structures. The details of the CEPRA technique and equivalent electrical circuit models will be discussed in this paper. Laboratory and

[1] Department of Civil Engineering, University of New Brunswick, Fredericton, NB, E3B 5A3, Canada; 0000-0002-6210-2390
[2] Giatec Scientific, Ottawa, ON, K2H 9E8, Canada

finite element modeling results will be presented to compare the traditional corrosion rate measurement techniques with the CEPRA method.

Keywords

Corrosion-monitoring, rebar corrosion, concrete durability, non-destructive testing, connectionless corrosion-monitoring, CEPRA

Introduction

In recent decades, several non-destructive electrochemical techniques were developed to monitor the corrosion rate of steel embedded in concrete. Such techniques rely on the method of determining the polarization resistance of metallic electrodes subjected to an electrochemical potential excitation. The polarization resistance theory was coined by Stern and Geary [1] and has been widely used, since then, to monitor instantaneous corrosion rates. These techniques are based on the assumption that there is a linear relationship between a small polarization around the electrode's open-circuit potential ($\Delta E < 20$ mV) and the current required to induce this potential shift (ΔI). In such cases, the polarization resistance (R_p) is calculated as the ratio between the shift in potential, from open-circuit potential, to the polarizing current used to induce this potential shift. By determining R_p, the corrosion rate (i_{corr}), in $\mu A/cm^2$, can be calculated using the Stern and Geary equation shown in Eq 1 [1]:

$$i_{corr} = \frac{\beta}{AR_p} \tag{1}$$

where β is the Tafel constant (in mV), A is the area polarized by the applied current (in cm^2) and R_p is the ratio between the change in voltage to the change in current (in ohms).

The typical method of determining the polarization resistance includes connecting a device that uses one of the potential-perturbing methods (e.g. the potentiostatic technique) to the rebar network. This is done through inducing damage to the concrete cover in order to establish such a connection. The aforementioned device then measures the electrode's open-circuit potential and applies a certain prespecified amount of current, or a potential shift, to polarize the reinforcement network. Subsequently, the potential response following the application of this polarizing current is monitored and fitted to the theoretical response of circuits representing the reinforced concrete system (typically the Randles circuit), in order to determine the polarization resistance. This method has been frequently applied in laboratory studies and research applications [2-5]. However, it has not been widely used for field applications among the civil engineering community due to the following reasons: (1) the concrete cover has to be damaged in order to establish a connection to the rebar network (2) the polarized area has been a large source of uncertainty, even with the use of the so-called guard-ring electrodes; especially in cases of macrocell corrosion and passive reinforcements [6-9] (3) a number of these techniques, such as electrochemical impedance spectroscopy (EIS), are very time consuming (4) Existing techniques that do not require a long measurement time (e.g. certain commercial devices implementing the galvanostatic pulse technique with a measurement time of 10 seconds) do not provide reliable results for the passive cases, due to the large time required for passive electrodes to reach quasi-steady-state conditions [10].

In recent years, a number of studies have observed that the reinforcement network can be polarized through the application of an external polarization such as that typical of the case of using a Wenner array probe in the vicinity of a reinforcement [11-14]. The earliest work on this method was reported by Monteiro, Morrison and Frangos [11], in which the authors demonstrated that when an experimental setup similar to that of a Wenner probe is used, in the reinforcement vicinity, and the applied current from the two outer probes is swept from very high to very low frequencies, the frequency-dependent characteristics of the interface are reflected in the complex ratio of potential difference between the inner electrodes to the applied current. This was supported by work in [12, 15, 16], in which results that were qualitatively similar to those obtained by classical EIS measurements, were obtained using this connectionless method. However, these studies also showed that the results obtained through such a method do not directly reflect the actual impedance of the system. The obtained results were found to be directly affected by the relative direction between the Wenner array and the reinforcing bar, the probes' spacing, the concrete cover depth and the concrete resistivity [12, 15, 16]. This is simply since a portion of the current, applied by the outer probes of the wenner array, flows explicitly through the electrolyte/concrete and another portion polarizes the reinforcement. The current polarizing the reinforcement depends on the aforementioned factors and cannot be directly determined. Furthermore, the obtained potential difference between the two inner probes, in such a setup, is not directly the potential shift exhibited by the working electrode. Several studies [13, 14, 17] have shown that the polarization resistance can be obtained, through such a method, if the concrete resistivity is known. This is since a knowledge of the concrete resistivity provides a measure of the amount of current flowing explicitly in the electrolyte/concrete as opposed to that polarizing the electrode.

The Connectionless Electrical Pulse Response Analysis (CEPRA) Technique

Although the aforementioned studies clearly indicate the applicability of this method, the experimental and analytical procedures used in the CEPRA technique are rather different. In typical DC measurements of the polarization resistance, the steel-concrete system is represented, simplistically, as a Randles circuit. If an AC current, at a wide range of frequencies, is applied to this circuit (similar to typical EIS measurements) and the potential response is monitored, then the circuit components can be analyzed by observing the changes in real impedance, imaginary impedance and phase shifts [6]. In the case of the Randles circuit, in the very high frequency range, the impedance caused by the double-layer capacitance tends to reach negligible values, and this double-layer acts as a short-circuiting element, leading to most of the current flowing through the electrolyte/concrete resistance and the short-circuit caused by the double-layer capacitance. Therefore, at the very high frequency ranges, the electrolyte/concrete resistance can be measured directly as the impedance modulus. At the very low frequency ranges, the impedance caused by the double-layer capacitance tends to reach very high values, leading to most of the current flowing through the electrolyte/concrete resistance and the polarization resistance. Therefore, at the low frequency range, their summation can be found directly as the impedance modulus.

In the connectionless technique, there is a higher system complexity. If a current pulse or a step voltage is applied from one of the two outer probes of a wenner probe, this current has two primary flow paths. One path is normal to the metallic electrode, which causes the charging of the double-layer capacitance or the polarization of the electrode (depending on the frequency of the applied current) and another path that is parallel to the metallic electrode, in which the current applied by one of the probes is consumed by the other. The portion of current flowing in each of these paths is dependent on the applied current's frequency, the concrete cover characteristics (cover depth and resistivity), the polarization resistance value, the rebar diameter and the double-layer capacitance. These are all interrelated factors that affect the current flow path and the obtained results. This system can be represented schematically using the circuit model shown in Fig. 1.

In this case, R_{c1} represents the probes' contact resistance and all of the current is faced by this resistance. This approach clearly identifies the two major current flow paths in the concrete medium through R_{c2} and R_{c3}, where R_{c2} represents the current flow path between the two probes (the path not polarizing the rebar) and R_{c3} represents the current flow path that polarizes the rebar or charges the double-layer capacitance. The magnitude of current passing by each of these resistors is dependent on: (1) the magnitude of their resistance (2) the impedance caused by the capacitance or the extent of charging of this capacitance (3) the magnitude of the polarization resistance (4) the concrete cover depth and reinforcement diameter (5) the frequency of the applied current. This circuit can be solved in order to determine the polarization resistance (R_{c4} in Fig. 1), if the current applied from the two outer probes is swept from very high to very low frequencies. However, this is a very time-consuming measurement that may take several minutes to a few hours depending on the circuit's time constant. Alternatively, the components of this system can be retrieved if the response (i.e. voltage difference between the two inner probes) to a narrow DC/AC current or voltage pulse applied from the outer probes for a short period of time is fitted to the theoretical transient obtained from this circuit. In these cases, the measured voltage response as a factor of time is similar to that of a charging RC circuit, shown in Eq 2, assuming that the electrolyte/concrete capacitance is negligible (same assumption as that in all of the other monitoring techniques)

$$V_{in}(t) = V_{ex}(A - Be^{-Dt}) \qquad (2)$$

where V_{ex} is the constant voltage applied through the external electrodes and V_{in} is the potential difference between the two inner electrodes.

The model shown in Fig. 1 was solved in order to determine the variables A, B and D. It was found that these variables follow functions shown in Eqs 3, 4 and 5. By measuring the voltage response over time, A, B and D can be calculated by fitting Eq 2 to the measured data. These factors can then be used to calculate the circuit components shown in Fig. 1. This solution approach is rather complicated compared to the Randles circuit used by all of the other techniques, or that used in [13]. However, such a circuit can be solved, just like any other, using more complicated solution procedures; if the cover depth is known. This is since the cover depth provides an indirect measure of the ratio of current flowing through R_{c2} to that flowing through $R_{c3.}$

$$A = f\left(R_{c1}, R_{c2}, R_{c3}, R_{c4}\right) \qquad (3)$$

$$B = g\left(R_{c1}, R_{c2}, R_{c3}, R_{c4}\right) \qquad (4)$$

$$D = h\left(R_{c1}, R_{c2}, R_{c3}, R_{c4}, C_{dl}\right) \qquad (5)$$

The commercial device used to implement this technique uses a four-probe Wenner array with an electrode spacing of 5 cm. The outer probes are used to apply a narrow DC/AC step voltage for a short period of time (6 seconds in this study) and the potential difference between the two inner probes is simultaneously monitored with a relatively high sampling rate. The current applied in this setup is typically in the range of 0.5 to 2 mA (note that this is not the polarizing current, since a large portion of this applied current flows explicitly inside the concrete between the two outer probes, as demonstrated later). The obtained transient is then fitted to Eq 2 to yield the constants A, B and D, which are used to calculate the system components shown in Fig. 1.

Experimental Methods

A total of 16 reinforced concrete blocks were cast for this portion of the study. The blocks, presented in Fig. 2, were each 300 mm (L) x 300 mm (W) x 100 mm (H) and reinforced with two black steel reinforcements at the same cover depth. The concrete mix design used is shown in Table 1. This mixture was selected to obtain a relatively high corrosion activity on the reinforcements in a short time, due to the higher permeability and lower resistivity of this concrete. Four dosages of admixed chlorides were used in this test to provide a wide range of corrosion activity and concrete resistivity. The admixed chloride dosages were 0%, 1.5%, 3% and 6% by weight of cement. For each of the admixed chloride percentages, four blocks were cast with the mix design shown in Table 1. Three of these blocks had rebars at different cover depths (each block had two reinforcements at either 20 mm, 40 mm, or 70 mm cover depth) in which 10M rebar was used (nominal diameter = 11.3 mm). For the fourth block, 20M rebar (nominal diameter = 19.5 mm) was used with 40 mm of cover depth to study the effect of reinforcement area on the results.

Thirty-two reinforcements were prepared for this study for the 16 blocks outlined. The end 3 cm of the reinforcements were epoxy-coated to prevent atmospheric corrosion and contamination, from the exposure to the atmosphere at the part of the reinforcement protruding from the concrete. The reinforcements were then thoroughly sandblasted to remove any prior corrosion by-products or mill scale. Finally, all of the reinforcements were weighed and the weight was recorded to the nearest 0.01 g.

Four molds were prepared allowing for the 3 blocks with different cover depths and the block with 20M reinforcement to be cast at once with the same concrete mixture. Four concrete mixtures, as those shown in Table 1, were conducted with each mix incorporating a different percentage of admixed chlorides (0%, 1.5%, 3% and 6% by weight of cement). The concrete was cast in accordance with ASTM C192. Casting was done in two layers, with each layer tamped for 30 times. The surface was finished using a steel trowel, and specimens were covered with wet burlap and wrapped in plastic for 24 hours. Specimens were then removed from the formwork after 1 day, and placed into a sealed container with an approximately 3-cm-deep layer of water to ensure the availability of the required moisture for corrosion propagation.

Weekly corrosion rate measurements were done on all of the slabs using the CEPRA technique. After 7 months, the specimens were removed from the containers and left to dry for a month during which measurements were conducted weekly to analyze the effect of the increased resistivity on the results. At the end of the exposure period (a total of 8 months), reinforcements were extruded by inducing a longitudinal crack along the reinforcement using a jackhammer. The mass loss of the reinforcements was found according to the ASTM G1, *Standard Practice for Preparing, Cleaning, and Evaluating Corrosion Test Specimens*, procedure C.3.5.

Finite Element Modeling

In order to study the current propagation behavior and the time-dependent potential response during the application of the CEPRA technique, a finite element model was developed. This section deals with the model formulation, constitutive relationships, input parameters and parameters studied.

Constitutive Relationships

In order to model the polarization behavior of the reinforcement, Faradaic and capacitive processes were assumed to apply at the steel surface. The electrochemical Faradaic kinetics governing the polarization behavior occurring at the steel-concrete interface can be modeled with the use of Butler-Volmer equation, shown in Eq 6 [18]:

$$j = j_o\left(10^{\frac{\eta}{b_a}} - 10^{\frac{-\eta}{b_c}}\right) \qquad (6)$$

where j is the net current density, j_o is the exchange current density, η is the change in potential (Φ) from the equilibrium potential (Φ_{eq}) of the electrode ($\Phi-\Phi_{eq}$), b_a is the anodic tafel coefficient and b_c is the cathodic tafel coefficient.

The effects of the charge-storage process (caused by the double layer capacitance) can be incorporated to the model assuming that the electrode surface behaves as a perfect capacitor during the charge storage or release process. The corresponding current charge/discharge at any time for such a capacitor can be represented as shown in Eq 7 [19]:

$$j_{cap} = C_{dl}\frac{\partial E}{\partial t} \qquad (7)$$

where C_{dl} is the electrode's double-layer capacitance and ∂E/∂t is the change in potential with respect to time.

Using this approach, the current at the steel-concrete interface after the application of a polarizing current is the sum of the Faradaic process (Butler-Volmer kinetics) and the capacitive currents. The total time-dependent current can then be expressed as shown in Eq 8 [19]:

$$j = j_o\left(10^{\frac{\eta}{b_a}} - 10^{\frac{-\eta}{b_c}}\right) + C_{dl}\frac{\partial E}{\partial t} \qquad (8)$$

In order to solve for the potential and current density distribution at the surface of the reinforcement, assuming electrical charge conservation and isotropic conductivity, ohm's law, shown in Eq 9, and charge conservation law, shown in Eq 10, are used for the concrete domain; assuming that concrete is a homogeneous medium with a uniform electrical resistivity [20]:

$$j = \frac{-1}{\rho}\nabla E \qquad (9)$$

$$\nabla j = 0 \qquad (10)$$

where j (A/m^2) is the current density, ∇E is the potential gradient and ρ is the resistivity of concrete (ohm.m).

Finite Element Modeling Procedure

The 3D simulations were performed using a COMSOL 5.2 software package. The domain of the problem, shown in Fig. 3, was chosen to represent a reinforced concrete member of 1 m in length, 0.3 m in width and 0.2 m in height, with a rebar embedded at a certain cover depth (variable parameter). At the steel-concrete interface (boundary a), Eq 8 was used as a Dirichlet-type boundary condition to find the time-dependent polarization behavior of the electrode. In the concrete domain (domain b), Eqs 9 and 10 were used in order to solve for the potential and current density distributions. External boundaries (boundary c) were modelled as electrically-insulated boundaries (Neumann boundary conditions with a specified normal current of zero). The CEPRA technique was modeled as Wenner array, with 4 probes having a probe spacing of 50 mm, in which the two outer probes were used to apply a current of 0.5 mA and -0.5 mA. The potential difference between the two inner probes was recorded as in the CEPRA technique. The four probes were modeled as perfect point objects.

Solutions were performed using a MUMPS solver (Multifrontal Massively Parallel Sparse direct Solver) inputted in the software. This solver makes use of the multifrontal method Gaussian-elimination and is based on the LU decomposition matrix-solving procedure. It should be noted, however, that other solvers available in the software were tried and their solutions were identical for the problem under consideration. However, the primary difference was the convergence time. The relative tolerance used was 0.001

In such a system, the summation of the current at the reinforcement surface and at the two current-applying electrodes is expected to be zero. This was used in order to discretize the mesh and minimize errors due to mesh elements' size and approximations [21]. This was conducted by trying several different mesh combinations for the concrete domain and the three different boundaries shown in Fig. 3, until the summation of current was negligible (less than 0.1% of the applied current). It was found that the optimum mesh configuration varies highly depending on the cover depth (due to the distance between reinforcement-surface boundary and external boundary) and concrete resistivity (due to potential gradients being different in high resistivity systems compared to low resistivity systems), among other factors.

Model Inputs and Investigated Parameters

The model was solved for cases representing passive reinforcements and cases representing actively corroding reinforcements. This was done by changing the input parameters in the Butler-Volmer equation according to Table 2. The anodic and cathodic beta coefficients for the active case were chosen to yield a beta coefficient of 26 mV; which is the value typically used for corrosion in reinforcing steel studies [22]. The exchange current density for the active case was adapted from that used by Marchand et al. [23] for the same purpose of this study. However, the effect of this parameter will be studied separately. The exchange current density for the passive cases was adapted from the model outlined in [20]. The beta coefficients for the passive case were chosen to yield a beta coefficient close to 52 mV; which is the value typically used for corrosion of reinforcing steel studies [22]. The anodic beta coefficient for the passive case also reflects passivation control and the ineffectiveness of anodic potential polarizations in increasing the anodic current for the passive case. This number is based on the mean value obtained in experimental work done by the authors; which will be presented in subsequent paper. The equilibrium potentials were obtained from [20]. However, it should be noted that this assumed potential has no effect on the trend of obtained results. For each of the passive and active cases, the parameters were studied as shown in Table 3.

Experimental Results

Figure 4 presents the weighted average corrosion rate determined by the CEPRA technique plotted versus the actual corrosion rate obtained by determining the mass loss. The actual corrosion rate was obtained using ASTM G1 procedure. The average electrochemically predicted corrosion rate was obtained by integrating the corrosion rates obtained by the technique throughout the monitoring period divided by the total period of exposure (8 months). Note that the measurements labelled dry are the average of measurements conducted during the drying month mentioned earlier, on specimens with no admixed chlorides. The dashed lines show the range of correlations accepted in the literature [2].

The results clearly indicate the applicability of the use of the technique to measure corrosion rates. For the actively corroding specimens (specimens with admixed chlorides), the predicted corrosion rates generally agreed well with the actual corrosion rates. Results for 21 out of 24 specimens fell in the range of results typically accepted in the literature; which is 0.5 to 2 times the actual corrosion rates [2]. The 3 specimens that did not fall in the typically accepted range still showed corrosion rates that were 0.35 to 0.45 times the actual corrosion rate, which is close to the lower accepted range. This correlation is similar, if not better, than those typically reported for well-established corrosion monitoring techniques applied for steel in concrete [24-28], especially for cases of low resistivity [26]. The success of the outlined method did not show to be affected by the reinforced concrete system characteristics in this case. This correlation was obtained similarly for a wide range of resistivities (obtained using different admixed chloride percentages), cover depths or reinforcement diameters.

For the passive specimens (specimens without admixed chlorides) in the dry condition, the results showed corrosion rates in the range of 0.2 $\mu A/cm^2$ or less; which is in the range that is typically accepted in the literature for passive reinforcements [10, 24, 27]. The same reliability in determining passive corrosion rates was obtained for the case of saturated concrete with 20M reinforcements. It has to be noted that this success in determining corrosion rates for passive reinforcements was obtained with a measurement time of only 6 seconds; which is much lower than the typical time required for other techniques for passive conditions [10]. This is due to the effect of this technique in shortening the time to steady-state conditions, as demonstrated further through modeling results, and due to using an exponential curve-fitting procedure used.

An overestimation of passive corrosion rates was found for the case of saturated specimens with 10M reinforcements; where the results fall in the range of 0.6 to 0.8 μA/cm^2. This is relatively higher than the range of corrosion rates expected for specimens without admixed chlorides, but is similar to results obtained for galvanostatic devices using short measurement times and non-modulated confinement [10, 27], and still allows differentiating passive and active reinforcements. It should be noted that the specimens showing 0.6-0.8 μA/cm^2 in saturated conditions started to show results lower than 0.4 μA/cm^2 after 1 day of drying, which represents cases of semi-saturated concrete that better resemble field cases (note that in the saturated condition, these specimens were not allowed to dry since casting). The substantial difference between the results obtained in the dry and saturated conditions is expected and will be discussed further through modeling results. It will be demonstrated, through modeling, that this only occurs for cases of saturated, low-resistivity, concrete with small-diameter reinforcements and it will be shown that the case used in this study (concrete with W/CM of 0.6 in saturated conditions reinforced with 10M rebar) served as a worst-case scenario compared to cases available in the field. This is evidenced by the good estimation of passive corrosion rates for dry, or semi-saturated, concrete and for reinforcements with larger diameters in saturated concrete; which better represent field conditions.

Finite Element Modeling Results

Figure 5 shows modeling results on the effect of concrete resistivity, cover depth, reinforcement diameter and exchange current density, on the current distribution on the rebar surface, for the case of actively corroding reinforcements. The base case was for a cover depth of 40 mm, a resistivity of 40 ohm.m, a reinforcement diameter of 10 mm and an exchange current density of 0.1 A/m^2. Each of the parameters was swept, from the base case, as shown. The presented results are all obtained at steady-state (at a time long enough that the double-layer capacitance is charged). The negative sign indicates anodic polarization while the positive sign indicates cathodic polarization.

The resistivity was found to influence the amount of current reaching the reinforcement in the range of low resistivities (20 ohm.m to 200 ohm.m), where more current polarizes the reinforcement area as resistivity increases. However, in the range of higher resistivities (higher than 200 ohm.m) there was little to no influence of resistivity on the current reaching the reinforcement. The effect of resistivity on the polarizing current is simply due to the availability of two current-consumption boundaries in this technique, as opposed to one in typical three-electrode LPR techniques. In typical techniques, any current that is applied by the counter electrode is consumed by the reinforcement; if current leakage/storage are considered negligible at steady-state. In the CEPRA technique, if a certain amount of current is applied from the positive (anodic) probe, it can be either consumed by the negative (cathodic) probe or in polarizing the reinforcement. As the resistivity between the two current-applying/receiving probes increases, more current preferentially flows to the reinforcement, instead of flowing between the two probes. Therefore, the current reaching the reinforcement increases as the resistivity increases. However, the polarized area shown by the technique is not strongly dependent on resistivity and confinement happens for all of the resistivities; which is very different from typical galvanostatic techniques in which confinement was found to be highly dependent on resistivity [7, 29, 30]

The effect of the cover depth showed that the current reaching the reinforcement was found to decrease as the cover depth increases. This is, simply, since larger concrete covers allow for a larger area for the polarizing current to flow between the two current-applying probes instead of polarizing the reinforcement. For lower covers, the current preferentially polarizes the reinforcement instead of flow in the electrolyte/concrete. The effect of the cover depth on the polarized area shows that lower covers lead to lower polarized areas and more localized polarization under the probe, while higher covers lead to more dispersion of the applied current in the concrete cover; which is in agreement with the effect observed for other corrosion-monitoring techniques [6, 7]. This may explain the reason for the underestimation of the corrosion rate for one of the 20 mm cover depth reinforcements when assuming that the full reinforcement is polarized. The same trend is observed for the effect of the reinforcement diameter. As the reinforcement diameter increases, more current can reach the reinforcement due to a higher electrode area available to consume this current. It seems that the area polarized by the technique tends to slightly decrease as the reinforcement diameter increases; due to the higher current consumption area available, which decreases the ability of the lateral propagation of the polarizing current. This may explain the underestimation of corrosion rate found for 2 of the 20M-reinforcement specimens.

The influence of exchange current density, or equivalently the polarization resistance, on the area polarized by the technique is very similar to that observed for resistivity. This is since the portion of current flowing in the path polarizing the reinforcement, as opposed to that parallel to the reinforcement, is determined by the relative values of concrete resistivity and polarization resistance; where lower polarization resistances encourage more current to reach the

385 reinforcement instead of flowing explicitly in the concrete. Nevertheless, the polarized area
386 shown by the technique is not strongly dependent on polarization resistance (in the range of
387 active corrosion rates) and confinement happens regardless the polarization resistance value;
388 which is very different from typical galvanostatic techniques in which confinement was found to
389 be highly dependent on the polarization resistance [7, 29].

390

391 Although the current reaching the reinforcement is variable, it is well estimated through
392 the model outlined in this paper; as evidenced by the accuracy of the technique for actively
393 corroding reinforcements. Furthermore, these results clearly indicate that the dependency of
394 confinement success on factors such as concrete resistivity, cover depth, reinforcement diameter
395 and exchange current density are very marginal and the polarized area changes with very low
396 magnitudes. The polarized length for this technique varied, for the cases shown and for other
397 cases not presented in this paper, for a wide range of concrete resistivities, cover depths,
398 reinforcement diameters and exchange current densities, from 50 cm (in cases of very large
399 cover depths and small reinforcement diameters) to 30 cm (in cases of very small cover depth
400 and large reinforcement diameters). This variance in polarized area is much lower than that
401 typically found for other techniques [7, 9, 30]. If, for instance, the polarized area is assumed to
402 be 40 cm for all of these cases, the error due to this assumption will not exceed 25%. This ability
403 to confine the polarized current, without the use of confinement techniques, stems from the
404 current-regulating nature of this technique, where the current reaching the reinforcement is
405 variable and depends on characteristics of the steel-concrete system. This is very different from
406 the currently-used techniques where confinement is essential. For instance, it has been shown
407 that achieving confinement, using the guard-ring technique, is very challenging in very low

resistivity systems, due to the higher tendency of the polarizing current to disperse laterally [7, 26]. This effect does not occur in the CEPRA technique since the current reaching the reinforcement decreases as resistivity decreases; leading to a lower effect of resistivity on confinement success.

Figure 6 shows the effect of resistivity on current distribution for the case of a passive reinforcement. These results were obtained for a cover depth of 40 mm and a diameter of 10 mm. As demonstrated previously, higher resistivities generally lead to higher amounts of current reaching the reinforcement. For low resistivities (Fig. 6b), it was found that confinement occurs only in the branch of the reinforcement near the cathodic probe while the full reinforcement area near the anodic probe is polarized; up to 0.5 m in this case. This is simply due to the challenge of polarizing a passive electrode anodically. This due to the electrode’s very low exchange current density and the very high anodic tafel slope (due to passivation control) leading to the reinforcement having a very limited ability to consume the anodic polarizing current. On the other hand, for cathodic polarizations, passive reinforcements tend to become better current consumers since the cathodic tafel slope is much lower than the anodic one (if no diffusion limitation exists). This leads to a limitation of the model due to the lack of symmetry between the two sides of the reinforcements, which means that R_{c3} shown earlier will not be the same under the two probes (R_{c3} will be identical for both sides only if the anodic and cathodic beta coefficients are equal). In the case of high resistivity systems, the symmetry is restored and confinement occurs, which leads to a better estimate of passive corrosion rates; this can, partially, explain the better estimate of passive corrosion rates in cases of semi-saturated or dry concrete. This limitation of confining anodic polarizations for passive electrodes is similar for all the techniques using anodic polarizations [8, 29, 30].

It should be also noted that the model outlined herein assumes that high and low frequency current-propagation behaviors follow the same path. This is essential in applying the model successfully. Figure 7 shows the typical current-propagation path for the case of a passive reinforcement at the high-frequency range (1 μs after current application). This is the same path as that for high- and low- frequency responses for active reinforcements. These paths are identical to Fig. 7 and are, therefore, not presented herein. Figure 8 shows the typical current-propagation path for the case of a passive reinforcement, with low resistivity concrete (40 ohm.m), at the low frequency range (500 s after current application). As mentioned previously, the high and low-frequency paths are rather similar in cases of actively corroding electrodes (both similar to Fig. 7); which explains the validity of the model and the accuracy obtained through it. However, this is not the case for the passive reinforcement in low resistivity concrete; since in the high frequency portion, the reinforcement's double-layer acts as a relatively good current-consumer (causing a shot-circuit effect), while at the low frequency region, this reinforcement acts as a current insulator (due to the high R_p) and hardly any current polarizes the reinforcement. It is clear that in the low frequency ranges for the passive reinforcements, the electrode tends to encourage current flow in a different path than that for the high frequency response (around and beneath the reinforcement). The low and high frequency current paths will tend to become more similar, and subsequently provide better results, when the current polarizing the reinforcement in the low frequency range increases. This polarizing current increases as the electrode's area available for current consumption increases or as the system resistivity increases, which explains the good results obtained for the dry or semi-saturated (high resistivity) cases, as well as cases with large reinforcement diameters (these cases better simulate field conditions). This may indicate that the overestimation found in case of saturated, low resistivity, concrete with small diameter passive rebar is not characteristic of the technique and only occurs in such scenarios.

Figures 9 and 10 illustrate the potential difference between the two inner probes as a factor of time for a case of resistivity of 40 ohm.m, a cover depth of 40 mm and a reinforcement diameter of 10 mm for a passive and active rebar, respectively. It is clear that the technique substantially reduces the time to reaching quasi-steady-state conditions compared to other techniques [10, 24, 27]. A measurement time of 10 seconds was found to provide adequate information about the polarization behavior of the reinforcement up to capacitance values in the range of 1 F/m^2 for the passive case (88% of the steady-state polarization was achieved in 10 second), and 5 F/m^2 in the active case (91% of the steady-state polarization was achieved in 10 second). This has been a major challenge for determining the passive reinforcements corrosion rates [10], especially with the very low exchange current density assumed in this model (10^{-5} A/m^2). The shortening of the measurement time associated with this technique has been previously proven experimentally [12, 31], theoretically [31] and numerically by the current study. The primary reason for this is that the polarizing current is very low in the area found in the middle of the reinforcement. Another reason is the lower electrode area contributing to the polarization. This, however, changes if the resistivity reaches very high values, due to the higher current received by the reinforcement, where higher resistivities lead to higher times to quasi-steady-state conditions. This shortening of the time to steady-state conditions leads to the technique's ability to determine corrosion rates in the passive cases in very few seconds; as evidenced by the experimental results. Such a feature is not applicable for techniques with constant applied currents.

Conclusions

This paper outlined the theory behind the CEPRA technique and introduced its use. From experimental and numerical work investigating the mode of application and reliability of the technique, the following conclusions can be drawn:

- The technique showed an accuracy in estimating the corrosion rates for actively corroding reinforcements that was similar to other well-established techniques that require a reinforcement connection and a longer measurement time.
- The technique showed success in determining passive corrosion rates in the case of dry or semi-saturated, high-resistivity, concrete and in the case of large reinforcement diameters. However, the technique overestimated the corrosion rates for passive cases when testing saturated concrete with small reinforcement diameters.
- The CEPRA technique was found to decrease the time to steady-state conditions for passive reinforcements considerably.
- The polarized area for the CEPRA technique has shown to vary in lower magnitudes compared to other techniques, without the use of confinement techniques, due to the self-regulating current for this technique.

ACKNOWLEDGMENTS

The authors would like to acknowledge Dr. Michael Thomas, University of New Brunswick, for his contribution to the experimental study and Dr. O. Burkan Isgor, Oregon State University, for his help throughout the model development process.

REFERENCES

[1] Stern, M., and Geary A.L., "A Theoretical Analysis of the Shape of Polarization Curves," *J. electrochem. Soc.,* Vol. 104, 1957, pp. 56-63

[2] Alonso, C., Andrade, C., and Gonzalez, J.A., "Relation between concrete resistivity and corrosion rate of the reinforcements in carbonated mortar made with several cement types," *Cement and Concrete Research,* Vol. 18, 1988, pp. 687-698

[3] Glass, G. K., Page, C. L., Short, N. R., and Zhang, J.Z., "The analysis of potentiostatic transients applied to the corrosion of steel in concrete," *Corrosion Science*, Vol. 39, No. 9, 1997, pp. 1657-1663.

[4] Pech-Canul, M. A., and Castro, P., "Corrosion measurements of steel reinforcement in concrete exposed to a tropical marine atmosphere," *Cement and Concrete Research*, Vol. 32, No. 3, 2002, pp. 491.

[5] Andrade, C., Alonso, C. and Sarria, J., "Corrosion rate evolution in concrete structures exposed to the atmosphere," *Cement and Concrete Composites,* Vol. 24, No. 1, 2002, pp. 55-64.

[6] Kranc, S. C., and Sagüés, A. A., "Polarization current distribution and electrochemical impedance response of reinforced concrete when using guard ring electrodes," *Electrochimica Acta,* Vol. 38, No. 14, 1993, pp. 2055-2061.

[7] Wojtas, H., "Determination of corrosion rate of reinforcement with a modulated guard ring electrode; analysis of errors due to lateral current distribution," *Corrosion Science*, Vol. 46, No. 7, 2004, pp. 1621-1632.

[8] Poursaee, A., and Hansson, C. M., "Galvanostatic pulse technique with the current confinement guard ring: The laboratory and finite element analysis," *Corrosion Science*, Vol. 50, No. 10, 2008, pp. 2739-2746.

[9] Nygaard, P. V., Geiker, M. R., and Elsener, B., "Corrosion rate of steel in concrete: evaluation of confinement techniques for on-site corrosion rate measurements," *Materials and Structures*, Vol. 42, No. 8, 2009, pp. 1059-1076.

[10] Martinez, I., Andrade, C., Rebolledo, N. Luo, L. De Schutter, G., "Corrosion-lnhibitor Efficiency Control: Comparison by Means of Different Portable Corrosion Rate Meters," *Corrosion*, Vol. 66, No. 2, 2010.

[11] Monteiro, P. J. M., Morrison, H. F. and Frangos, W., "Nondestructive Measurement of Corrosion State of Reinforcing Steel in Concrete." *ACI Materials Journal*, 95, Vol. 6, 1998, pp. 704-709.

[12] Zhang, J., Monteiro, P. J. M. and Morrison, H. F., “Noninvasive Surface Measurement of Corrosion Impedance of Reinforcing Bar in Concrete-Part 1: Experimental Results,” *ACI Materials Journal*, Vol. 98, No. 2, 2001, pp. 116-125.

[13] Andrade, C., and Martínez, I., “Metal Corrosion Rate Determination of Different Solutions and Reinforced Concrete Specimens by Means of a Noncontacting Corrosion Method,” *Corrosion*, Vol.66, No.5, 2004.

[14] Keddam, M., Nóvoa, X. R., & Vivier, V., “The concept of floating electrode for contact-less electrochemical measurements: Application to reinforcing steel-bar corrosion in concrete,” *Corrosion Science*, Vol. 51, No. 8, 2009, pp. 1795-1801.

[15] Zhang, J., Monteiro, P. J. M. and Morrison, H. F., “Noninvasive Surface Measurement of Corrosion Impedance of Reinforcing Bar in Concrete-Part 2: Forward Modeling,” *ACI Materials Journal*, Vol. 99, No. 3, 2002, pp. 242-249.

[16] Zhang, J., Monteiro, P.J.M., Morrison, H.F. and Mancio, M., “Noninvasive surface measurement of corrosion impedance of reinforcing bar in concrete—part 3: effect of geometry and material properties,” *ACI Materials Journal*, Vol. 101, No. 4, 2004, pp. 273–280.

[17] Keddam, M., Nóvoa, X. R., Puga, B., & Vivier, V., “Impedance based method for non-contact determination of the corrosion rate in buried metallic structures,” *European Journal of Environmental and Civil Engineering*, Vol. 15, No. 7, 2011, pp. 1097-1103.

[18] Frankel, G.S., “Fundamentals of Corrosion Kinetics,” In: Hughes, A., Mol, J., Zheludkevich, M., Buchheit, R., (eds) *Active Protective Coatings*. Springer Series in Materials Science, vol 233, 2012. Springer, Dordrecht.

[19] Kranc, S., and Sagues, A.A., “Modeling the Time□Dependent Response to External Polarization of a Corrosion Macrocell on Steel in Concrete,” *J. Electrochem. Soc.*, Vol. 144, No. 8, 1997, pp. 2643-2652

[20] Pour-Ghaz, M., Isgor, O. B., and Ghods, P., “The effect of temperature on the corrosion of steel in concrete. Part 1: Simulated polarization resistance tests and model development,” *Corrosion Science*, Vol. 51, No. 2, 2009, pp. 415-425.

[21] Clement, A., Laurens. S., Arliguie. G., and Deby F., "Numerical Study of the Linear Polarisation Resistance Technique Applied to Reinforced Concrete for Corrosion Assessment," *European Journal of Environmental and Civil Engineering*, Vol. 16, No. 3-4, 2012, pp. 491-504.

[22] Andrade, C. and González, J.A., “Quantitative measurements of corrosion rate of reinforcing steels embedded in concrete using polarization resistance measurements,” *Mater. Corros.*, vol. 29, no. 8, 1978, pp. 515-519

[23] Marchand, J., Laurens, S., Protière, Y., Samson E., “A Numerical Study of Polarization Tests Applied to Corrosion in Reinforced Concrete”. *ACI special publication,* Vol. 312, 2017, pp. 1-12

[24] T. Luping, Calibration of the Electrochemical Methods for the Corrosion Rate Measurement of Steel in Concrete, *NORDTEST Project No. 1531-01*, 2005.

[25] Law, D.W., J. Cairns, S.G. Millard, and J.H. Bungey., "Measurement of Loss of Steel from Reinforcing Bars in Concrete Using Linear Polarisation Resistance Measurements," *NDT and E International*. Vol. 37, No. 5, 2004, pp. 381-388.

[26] Andrade, C., and Martínez, I., "Calibration by gravimetric losses of electrochemical corrosion rate measurement using modulated confinement of the current," *Materials and Structures*, Vol. 38, No. 9, 2004, pp. 833-841.

[27] Poursaee, A., "An analysis of the factors influencing electrochemical measurements of the condition of reinforcing steel in concrete structures," *PhD Thesis*, University of Waterloo, Waterloo, Ontario, Canada, 2007.

[28] Pradhan, B., & Bhattacharjee, B., "Performance evaluation of rebar in chloride contaminated concrete by corrosion rate," *Construction and Building Materials*, Vol. 23, No. 6, 2009, pp. 2346-2356.

[29] Flis, J., Sehgal, A., Li, D., Kho, Y., Sabotl, S., Pickering, H., Osseo-Asare, K. and Cady, P.D., "Condition Evaluation of Concrete Bridges Relative to Reinforcement Corrosion Volume 2: Method for Measuring the Corrosion Rate of Reinforcing Steel," *Strategic Highway Research Program,* Washington *DC*, 1993.

[30] Mitzithra, M.E., "Detection of corrosion of reinforced concrete on cooling towers of energy production sites," *PhD Thesis*. Universite De Toulose, Toulose, France, 2013.

[31] Lim, Y. C., Noguchi, T. and Shin, S. W., "Formulation of a Nondestructive Technique for Evaluating Steel Corrosion in Concrete Structures," *ISIJ International*, Vol. 49, No.2, 2009, pp. 275-283

TABLE 1 Mix design used for the laboratory test blocks

Constituent	Amount, kg/m^3
GU Cement	265
Coarse Aggregate (<19 mm)	1055
Fine Aggregate	940
Water	165

TABLE 2 Model inputs for active and passive cases

Input	Passive case parameters	Active case parameters
j_o	10^{-5} A/m^2	0.1 A/m^2
b_a	5 V	0.12 V
b_c	0.12 V	0.12 V
Φ_{eq}	0.16 V	-0.78 V
C_{dl}	Variable	Variable

TABLE 3 Parameters investigated

Independent Variable	Cases
Cover depth	20, 40, 70 and 100 mm
Resistivity	20, 50, 100, 200, 500 and 1000 ohms.cm
Reinforcement diameter	10, 20 and 30 mm
i_o (for the active case)	0.01, 0.05, 0.1, 0.5 A/m^2

List of Figure Captions

Fig. 1 Circuit model used to represent the CEPRA technique

Fig. 2 Schematic representation of the test blocks

Fig. 3 Domain of the finite element model: (a) reinforcement surface, (b) concrete domain, (c) external boundaries, (d) Wenner probe

Fig. 4 Results obtained from the CEPRA technique compared to the actual corrosion rate (a) as a factor of admixed chloride percentage and (b) as a factor of cover depth and reinforcement diameter

Fig. 5 Effect of (a) resistivity, in ohm.m, (b) cover depth, in m, (c) rebar diameter, in m, (d) exchange current density, in A/m^2, on the distribution of polarizing current for a uniformly corroding rebar

Fig. 6 Effect of resistivity, in ohm.m, on current distribution for the case of a passive rebar

Fig. 7 High frequency current path (evaluated 1 μsec after current application) for a case representing passive reinforcements (note that this is identical to the current path for high and low frequency responses for active reinforcements)

Fig. 8 Low frequency current path (evaluated at steady-state) for a case representing passive reinforcements in low resistivity concrete

Fig. 9 Effect of the double-layer capacitance, in F/m^2, on the obtained time-transient for the case of a passive rebar up to: (a) 100 seconds and (b) 10 seconds

Fig. 10 Effect of the double-layer capacitance, in F/m^2, on the obtained time-transient for the case of an active rebar up to: (a) 100 seconds and (b) 10 seconds

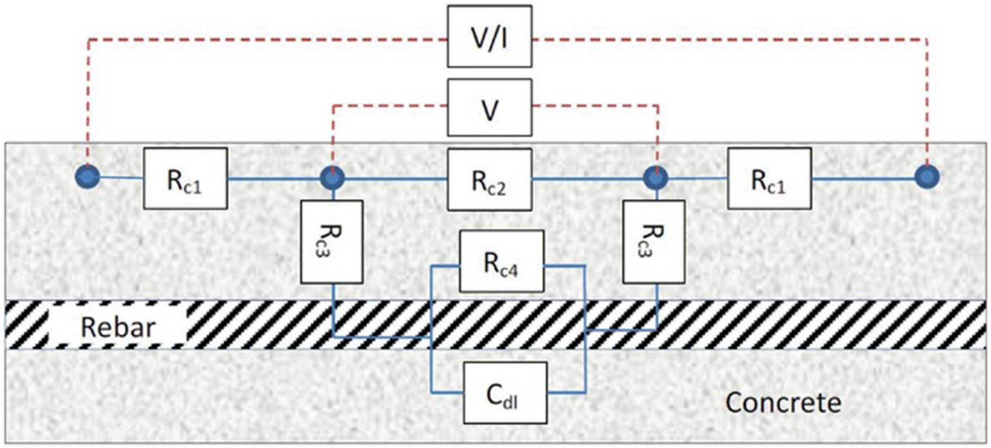

Fig. 1 Circuit model used to represent the CEPRA technique

57x26mm (300 x 300 DPI)

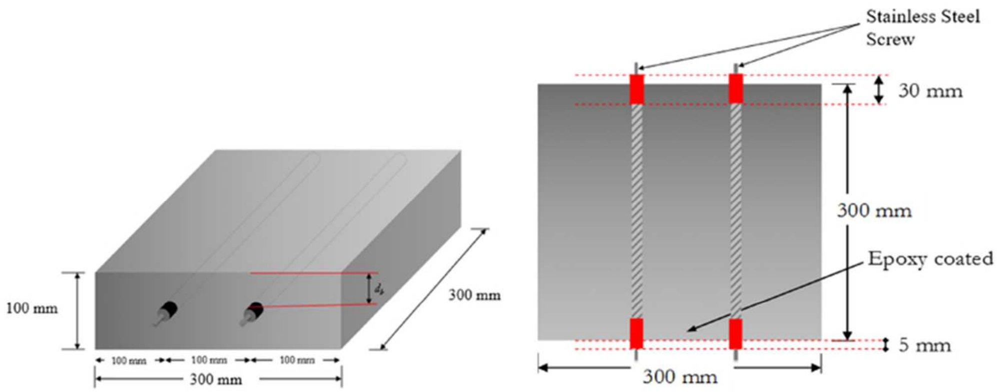

Fig. 2 Schematic representation of the test blocks

65x26mm (300 x 300 DPI)

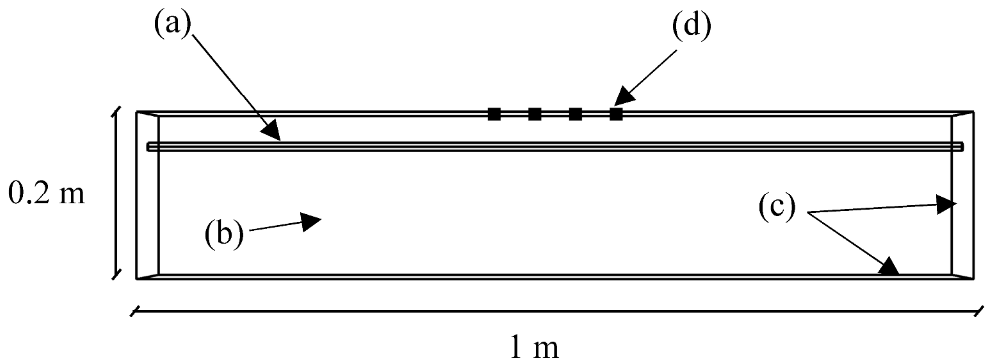

Fig. 3 Domain of the finite element model: (a) reinforcement surface, (b) concrete domain, (c) external boundaries, (d) Wenner probe

1067x423mm (96 x 96 DPI)

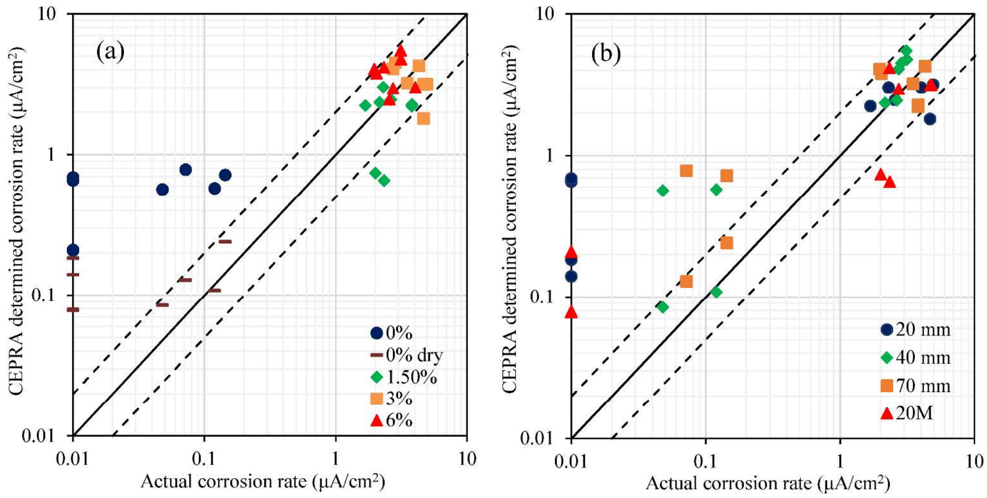

Fig. 4 Results obtained from the CEPRA technique compared to the actual corrosion rate (a) as a factor of admixed chloride percentage and (b) as a factor of cover depth and reinforcement diameter

976x501mm (96 x 96 DPI)

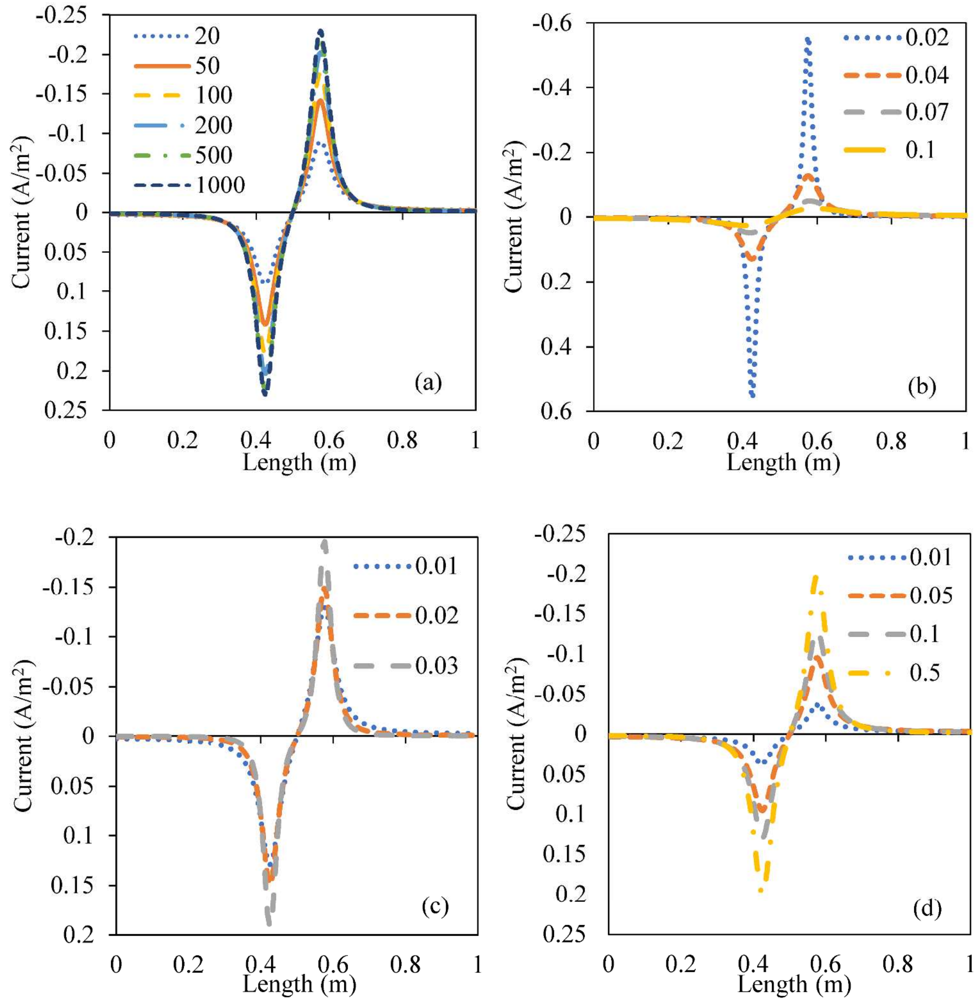

Fig. 5 Effect of (a) resistivity, in ohm.m, (b) cover depth, in m, (c) rebar diameter, in m, (d) exchange current density, in A/m2, on the distribution of polarizing current for a uniformly corroding rebar

1015x1035mm (96 x 96 DPI)

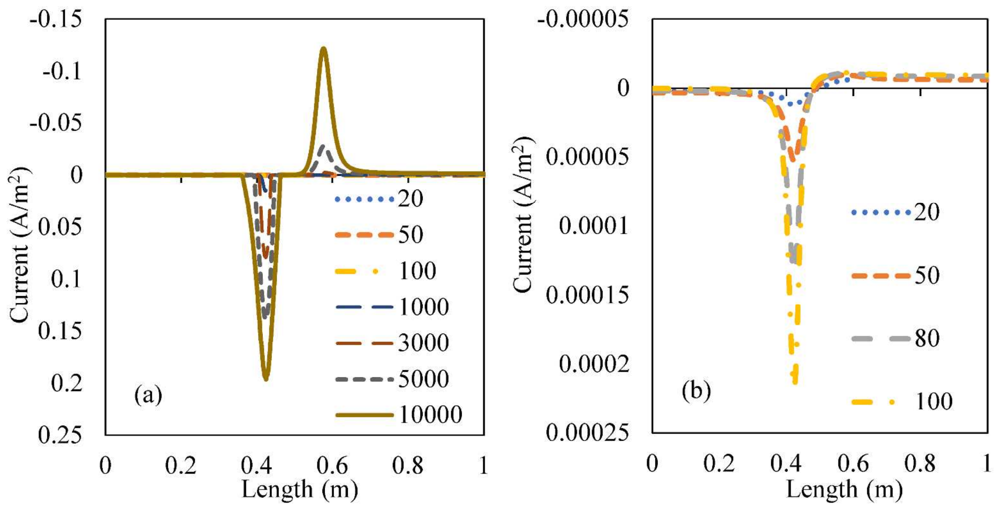

Fig. 6 Effect of resistivity, in ohm.m, on current distribution for the case of a passive rebar

992x501mm (96 x 96 DPI)

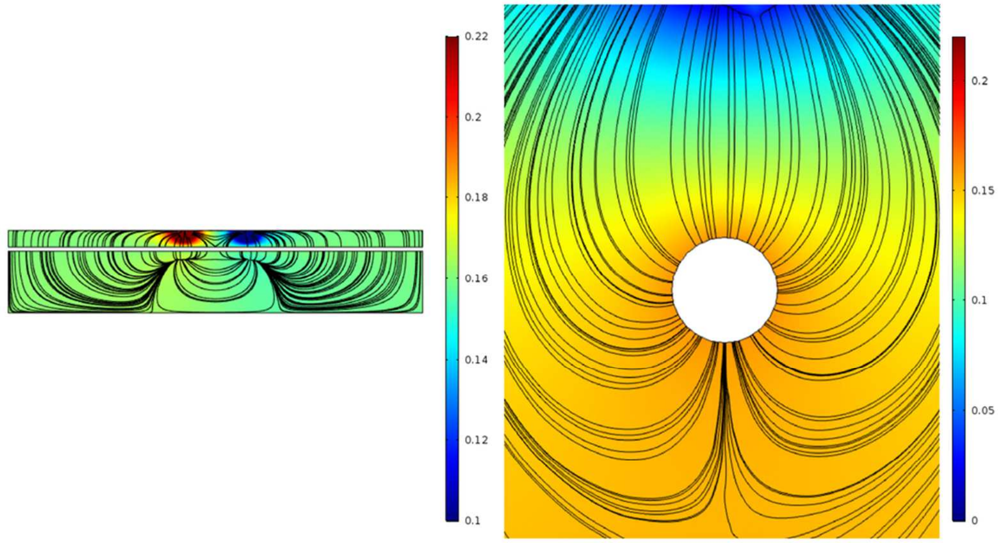

Fig. 7 High frequency current path (evaluated 1 μsec after current application) for a case representing passive reinforcements (note that this is identical to the current path for high and low frequency responses for active reinforcements)

87x48mm (300 x 300 DPI)

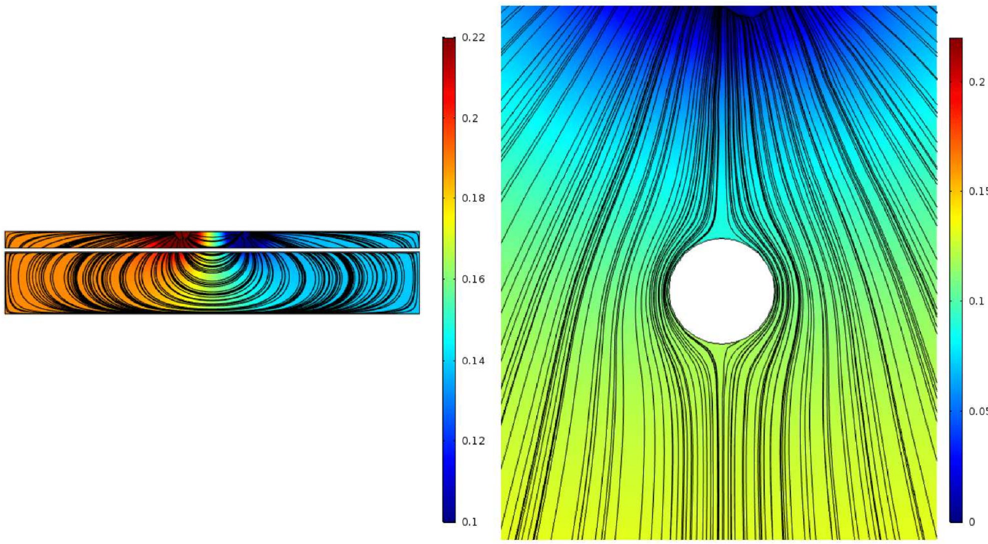

Fig. 8 Low frequency current path (evaluated at steady-state) for a case representing passive reinforcements in low resistivity concrete

986x543mm (96 x 96 DPI)

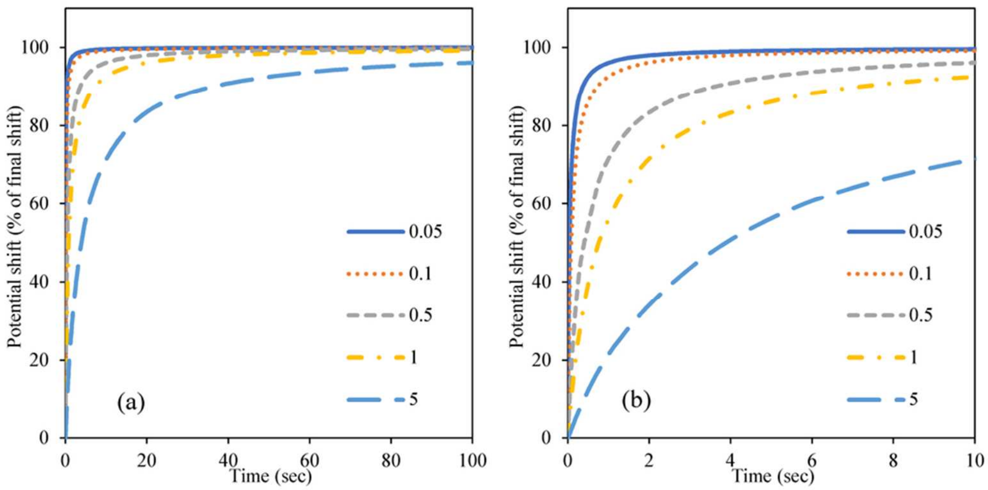

Fig. 9 Effect of the double-layer capacitance, in F/m2, on the obtained time-transient for the case of a passive rebar up to: (a) 100 seconds and (b) 10 seconds

81x41mm (300 x 300 DPI)

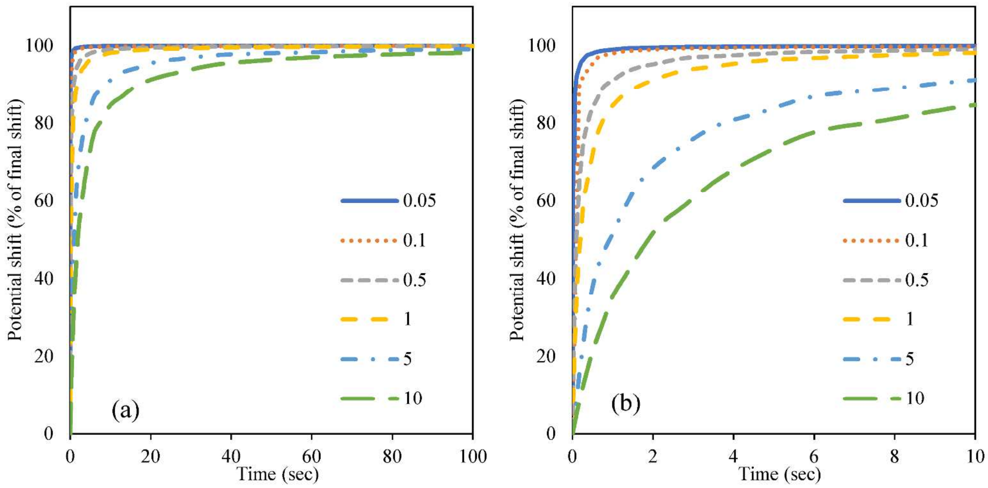

Fig. 10 Effect of the double-layer capacitance, in F/m^2, on the obtained time-transient for the case of an active rebar up to: (a) 100 seconds and (b) 10 seconds

996x511mm (96 x 96 DPI)